A design concept of parallel elasticity extracted from biological muscles for engineered actuators

2016 Bioinspir. Biomim. 11 056009

(http://iopscience.iop.org/1748-3190/11/5/056009)

Bioinspiration & Biomimetics

PAPER

A design concept of parallel elasticity extracted from biological muscles for engineered actuators

Jie Chen[1,2], Hongzhe Jin[1], Fumiya Iida[2] and Jie Zhao[1]

[1] State Key Laboratory of Robotics and System, Harbin Institute of Technology, Harbin 150001, People's Republic of China
[2] Department of Engineering, University of Cambridge, Cambridge CB2 1PZ, UK

E-mail: jchen@hit.edu.cn

Keywords: muscle elasticity, parallel elasticity, energy efficiency, disturbance rejection

OPEN ACCESS

RECEIVED
11 November 2015

REVISED
21 July 2016

ACCEPTED FOR PUBLICATION
22 July 2016

PUBLISHED
23 August 2016

Abstract

Series elastic actuation that takes inspiration from biological muscle-tendon units has been extensively studied and used to address the challenges (e.g. energy efficiency, robustness) existing in purely stiff robots. However, there also exists another form of passive property in biological actuation, parallel elasticity within muscles themselves, and our knowledge of it is limited: for example, there is still no general design strategy for the elasticity profile. When we look at nature, on the other hand, there seems a universal agreement in biological systems: experimental evidence has suggested that a concave-upward elasticity behaviour is exhibited within the muscles of animals. Seeking to draw possible design clues for elasticity in parallel with actuators, we use a simplified joint model to investigate the mechanisms behind this biologically universal preference of muscles. Actuation of the model is identified from general biological joints and further reduced with a specific focus on muscle elasticity aspects, for the sake of easy implementation. By examining various elasticity scenarios, one without elasticity and three with elasticity of different profiles, we find that parallel elasticity generally exerts contradictory influences on energy efficiency and disturbance rejection, due to the mechanical impedance shift thus caused. The trade-off analysis between them also reveals that concave parallel elasticity is able to achieve a more advantageous balance than linear and convex ones. It is expected that the results could contribute to our further understanding of muscle elasticity and provide a theoretical guideline on how to properly design parallel elasticity behaviours for engineering systems such as artificial actuators and robotic joints.

1. Introduction

Articulated systems commonly exist and are used in both the natural world (e.g. human beings and mammals) and the engineering domain (e.g. robotic arms/hands [1] and legged robots [2]). Typically these systems use joints, which are driven by biological or artificial actuators (e.g. muscles, electric motors), as fundamental 'units' to achieve desirable movements such as reaching, grasping and walking. As a result, the performance of the whole system is highly dependent on that of joints.

Biological joints use muscles as the source of force for movement [3] and accommodate external disturbances in two different ways: passive adaptation by intrinsic properties of biological components and active control by the central nervous system (CNS). The former is regarded as an effective supplement and solution to simplify and cope with the challenges (e.g. time delay, energy use and robustness) existing in the latter one. From this perspective, being the motor of biological joints, muscles' inherent elasticity should be extremely crucial for the remarkable dynamic performance of animals. It appears that nature has found an effective way to make the best use of this property of muscles after millions of years of evolution. As exemplified in figure 1, biologists have found, by measuring the passive force–length (elasticity) relationships in different frog muscles using laser diffraction techniques, a concave-upward or even exponential tendency [4–6]. Likewise, similar elasticity behaviours are also experimentally identified in the muscles of rabbits [7, 8], humans [9], etc. All this experimental evidence essentially reveals a universal preference in biological

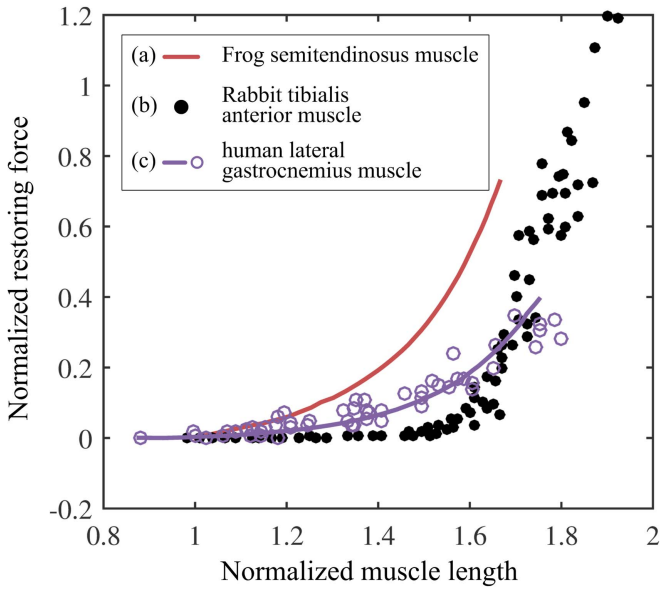

Figure 1. Elasticity behaviours (force–length relationships) in muscles of different animals. (a) corresponds to frog semitendinosus muscle; (b) represents the elasticity characteristic of rabbit tibialis anterior muscle; (c) is identified from the lateral gastrocnemius muscle of a human. All this experimental evidence suggests a universally concave-upward elasticity behaviour in biological muscles. Data from [5, 8, 9].

muscles. Furthermore, biomechanists have also pointed out that the output force for each muscle is the sum of an active component and a passive component [10], implying that muscle-like elasticity could be technically recreated in the form of parallel elasticity.

In engineering applications, roboticists have been attempting to integrate an elastic property into artificial actuators for the purpose of enabling engineered systems comparable to biological ones. Following this idea, series elastic structures that take inspiration from biological tendons have been extensively studied and used in today's robots. A representative physical realization is to combine mechanical springs in series with electric motors; namely, series elastic actuators (SEAs) [11, 12]. Many considerations go into the approach of achieving this elasticity through cable-driven actuations [13, 14]. Apart from those, we also noticed several other studies that have looked at the utilization of parallel elasticity, which can be thought to mimic the elastic property within muscles. For example, the authors of [15] investigated the effects of parallel elasticity using a 2-DOF robotic finger with extension springs. They found that the integration of parallel elasticity leads to improved stability and robustness in robotic hands during grasping and manipulation. The authors of [16] compared to a linear and a physiologically based parallel elasticity profile with a two-segment swinging robotic leg, and found that both can reduce the energetic cost of leg swinging through wisely choosing parameter values. A final example is [17], in which several cases without parallel springs and with parallel springs of different stiffnesses and preloads were studied with a planar bipedal robot. The authors found that the addition of springs in parallel with the knee actuators can improve the energetic efficiency of walking, with higher stiffness providing greater benefit at higher speeds and lower stiffnesses providing benefit at lower speeds. All these attempts have demonstrated the effectiveness of parallel elasticity to achieve robust and efficient movements.

Despite impressive achievements, it is still a common and somewhat intractable problem to emulate the elastic property of biological muscles, even for a single robotic joint. A significant challenge lies in determining the profile of elasticity. Obviously, the straightforward implementation of a muscle-like elasticity profile requires costly mechatronic design and, from our point of view, is not necessarily suitable due to the limits of current state-of-the-art technologies and the differences between biological and engineering systems. With these considerations in mind, the current paradigm is to use either a simple-to-design but not optimal-performance method of selecting a plausible elastic element (e.g. mechanical spring) from those commercially available off the shelf, or a better-performance but not versatile elasticity profile tailored to fulfill a specific task. In addition, there seems to be a consensus that nonlinear profiles of elasticity have a more positive effect than linear ones [18–20]. However, at present it is still open as to what type of nonlinearity is a good fit. In fact, to the best of our knowledge, there are very few studies in the literature to address how to reasonably copy the elastic property of biological muscles into artificial systems.

As a step towards further understanding the functions of muscle elasticity and more effectively applying this property in the engineering domain, this paper seeks to determine, through examination of a

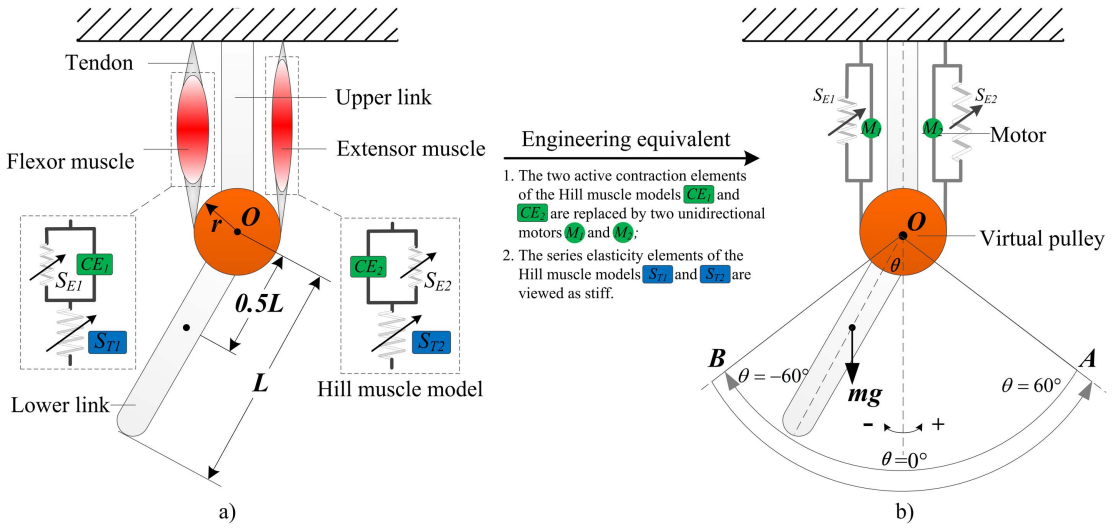

Figure 2. The conceptual joint model with parallel elasticity. (a) A relatively complete joint model with full Hill-type muscle components comprising active contraction activation *CE*, tendon-like elasticity S_T and muscle-like elasticity S_E. (b) A reduced joint model with a specific focus on the muscle elasticity aspect. Such simplification allows easy implementation without eliminating the elasticity characteristics that are of interest to our investigation.

conceptual joint model, the potential functional benefits behind the preferred elasticity profiles in biological muscles and to distill a general guideline for the engineering-applicable design of elasticity profiles. Firstly, a single-degree-of-freedom rotary joint model implementing periodic motions is developed, on the basis of analyzing the agonist–antagonist muscle configuration in biological joints. The elastic property of the muscle pair is seriously considered in this model. Then the effects of various elasticity profiles on two crucial but contradictory demands for artificial systems, energy efficiency and disturbance rejection, are compared and contrasted in detail, followed by an explanation of the mechanisms underlying the observed behaviours. Finally, several lessons that can be learned from this study are discussed.

2. Methods

2.1. The conceptual joint model with parallel elasticity

To explore the behaviour of parallel elasticity in detail, we consider a conceptual model with only one rotary degree of freedom, as illustrated in figure 2(a), which is the basic component of articulated systems. It consists of an upper segment and a lower segment (with mass m and inertia J) that is able to rotate around the upper one. For the actuation of this model, an antagonistic pair of muscles, similar to animal muscle actuation, is included. Both the extensor and flexor muscle are described by a Hill-type muscle model [21] which has been used as the conceptual foundation in biomechanical modelling.

Despite only a single-degree-of-freedom joint, it is still challenging to implement a systematic investigation with the developed model. This is because unlike existing studies that just choose muscle-tendon parameters based on biological data or empirical estimates, the primary objective of this study is to investigate the effects of various parallel elasticity behaviours by performing a parameter scan and to clarify possible design implications for parallel elasticity. With the actuation model in figure 2(a), however, a large number of parameters of muscle activation and tendon-like (series) elasticity would have to be estimated, in addition to those describing the muscle-like elasticity. This causes the analysis to be computationally difficult. On a deeper level, the muscle-tendon units of biological organisms are dynamically coupled and have already been well tuned through evolution to provide the desired superiority, like high efficiency and robustness. It is therefore very likely that the respective effects of muscle-like elasticity would be less marked or even eliminated if model parameters (of tendon-like elasticity) are not properly designed. With these in mind, we seek to reduce the model complexity without compromising the characteristics of parallel elasticity that are of our interest. Two following measures are taken: (I) two unidirectional motors are used as replacements for the two active contraction elements of the muscle pair, as illustrated in figure 2(b), which allows us to calculate the active forces simply using a Lagrangian approach without interfering with the complicated muscle activation and parameter tuning; (II) as a second approximation, tendon-like series elasticity is ignored in this work, taking account of the fact that: (1) tendons are another equally important elastic elements in biological joints, their elasticity profiles are also unknown, a full consideration of which would greatly complicate the whole investigation (a better approach is to study one element

while keeping others in a suitably simple setting); (2) the stiffness of a muscle is normally considerably less than the tendon stiffness [22–24], therefore tendons can be viewed to be stiff if no large perturbations (e.g. ground impact at touchdown) are involved during simulation; (3) researchers have argued that this simplification greatly facilitates the analytic process at the expense of a relatively small loss in accuracy [25, 26]. Simplifying by reducing the model dimensionality, we thus arrive at a simplified joint model[3] (figure 2(b)) that allows a systemic investigation and comparison of muscle-like parallel elasticity.

The equation of motion of this conceptual joint model can be expressed as

$$\tau_M + \tau_g + \tau_e + \tau_{ext} = I\ddot{\theta} \quad (1)$$

where τ_M is the torque provided by the two unidirectional motors. Here we ignore the complicated activation process and just calculate τ_M through equation (1); $\tau_g = \frac{1}{2}mgL\sin\theta$ is the gravitational torque; $\tau_{ext} = F_{ext} \cdot L$ is the torque provided by external forces; $I = \frac{1}{12}mL^2 + m\left(\frac{1}{2}L\right)^2 = \frac{1}{3}mL^2$ is the rotational inertia of the lower limb; and τ_e is the elastic torque from muscle elasticity and can be written as

$$\tau_e = f(\Delta l) \cdot r \quad (2)$$

where r is the radius of the virtual pulley, $\Delta l = \theta \cdot r$ is the deflection of the elastic element, $f(\Delta l)$ is the elastic force generated by parallel elasticity S_{E1} $(\theta > 0)$ or S_{E2} $(\theta < 0)$ (see figure 2), the function f could be linear or nonlinear. In this paper, $\theta = 0$ is set as the position of optimal length l_0 of the two muscles at which there is no passive restoring force, without consideration of the asymmetric structure existing in biological joints. With this setup, the elastic force always acts with gravity. We can derive from equation (1) that the profile of elasticity has a direct impact on the performance of the joint.

2.2. Modelling the parallel elasticity

The goal of this work is to draw possible design clues for parallel elasticity by performing an exhaustive search of its profiles. For a systematic search, four scenarios with different elasticity configurations are compared and contrasted. Scenario 1 is the simplest case, in which simulation is executed without elasticity, and with which other configurations can be weighed. In scenarios 2 through 4, three families of elasticity with distinct profiles are explored, respectively, as illustrated in figure 3. At a more detailed level, for a start, a family of linear elasticity with the force-deflection relationship $f = c_L\Delta l \quad (c_L > 0)$ is examined, where c_L is the linear coefficient, Δl is the spring deflection; especially we called this term, the ***linear term***. Then, as an extension, a ***nonlinear*** term $c_{NL}(\Delta l)^2$ is added, where c_{NL} is the nonlinear coefficient describing the concavity/convexity of the elasticity profiles. To generalize the results beyond a particular system, c_L and $c_{NL}$are normalized to link mass m, length L, gravitational acceleration g and the radius of the virtual pulley r through $C_L = c_L r^2/mgL$ and $C_{NL} = c_{NL} r^3/mgL$. In this regard, the elastic torque τ_e in equation (2) can be further expressed as

$$\tau_e = C_L\theta + C_{NL}(\theta)^2, \quad (3)$$

and also the four scenarios can be specified as follows:

- scenario 1: $C_L = 0$ and $C_{NL} = 0$;
- scenario 2: $C_L > 0$ and $C_{NL} = 0$, corresponding to linear elasticity;
- scenario 3: $C_L > 0$ and $C_{NL} < 0$, where the elasticity turns nonlinearly convex, revealing a softening elasticity characteristic;
- scenario 4: $C_L > 0$ and $C_{NL} > 0$. Here the elasticity turns nonlinearly concave, representing a stiffening elasticity characteristic;

So by scanning over the parameter space consisting of linear coefficient C_L and nonlinear coefficient C_{NL}, we are able to gain an insight as to how it could affect the joint performances and dynamic responses.

2.3. Performance metrics and simulation procedure

Being both ***robust to disturbances*** and ***energetically efficient*** is desirable for artificial machines, particularly for those robots expected to manipulate or locomote in complex environments such as disaster areas, dangerous regions and highly unstructured terrains. These two aspects are usually stated as the main concerns about using parallel elasticity in robotic joints: the parallel elasticity is able to share part of the actuator torque and thus helps reduce the active energy consumption, but it may also counteract the actuator torque sometimes; in turn, such counteraction can be beneficial to disturbance rejection, and the rapid mechanical feedback loop formed by elastic elements may further provide self-righting after perturbation [27, 28]. From this perspective, two subsequent stages are included in our simulation study, with the aim of examining the disturbance rejection and energy efficiency behaviours, respectively. During simulations, the joint was open-loop torque controlled, that is, no feedback control action was applied. The main reason for doing so is the specific purpose of this study: we wish to examine the respective influences of the changed joint dynamics itself, caused by various elasticity behaviours, on these two performance metrics. All simulations were run in MATLAB (R2014b, MathWorks Inc., Natick, MA, USA), and the

[3] The antagonistic configuration is reserved for a more straightforward correspondence with biological joints, even though it can be further reduced by replacing the unidirectional motors and elastic springs with bidirectional ones during engineering realization.

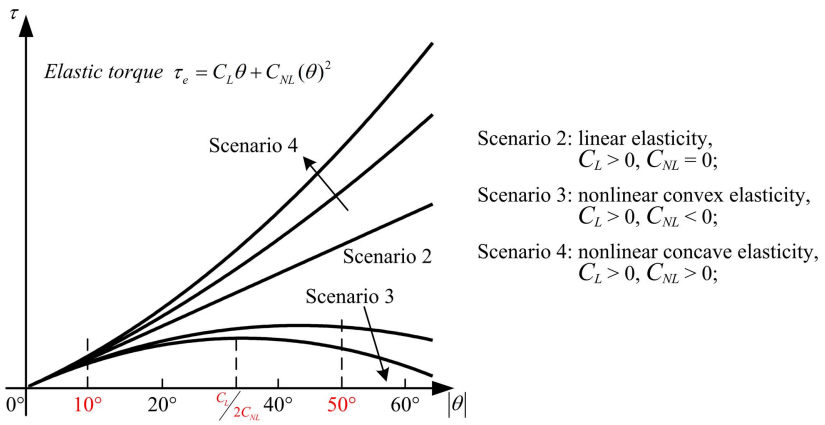

Figure 3. Scenarios 2 through 4 with different elasticity configurations. Scenario 2 is characterized by a series of linear elasticity $\tau_e = C_L\theta$; scenarios 3 and 4 are extensions of scenario 2 by adding the nonlinear term $C_{NL}(\theta)^2$, and correspond to $C_{NL} < 0$ and $C_{NL} > 0$, respectively.

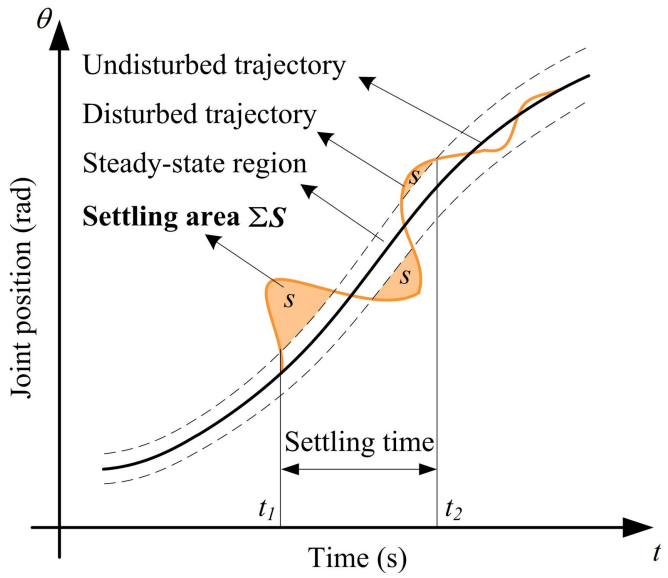

Figure 4. Schematic representation of settling area used to assess disturbance rejection. The black thick line represents undisturbed joint trajectory, the two dashed lines correspond to allowed steady-state boundary (5% in this work), and the orange line indicates disturbed joint trajectory which deviates due to external perturbations at time t_1 and returns to steady state at time t_2. So, settling time is (t_2- t_1), settling area is the area enclosed between two boundary lines and actual trajectory outside the steady-state region.

Runge–Kutta fourth order method (ode45) with a maximum time-step size of 0.01s was implemented to solve the system dynamics. An exhaustive search of elasticity profiles was performed during the simulation, with linear coefficient $C_L \in [0,0.07] \cdot mgL$ and nonlinear coefficient $C_{NL} \in [-0.05,0.05] \cdot mgL$.

2.3.1. Disturbance rejection

In the first stage, the joint was commanded to execute a periodic motion between position A and B (±60°, see figure 2) along a sinusoidal trajectory, during which an impulsive perturbation was applied to the joint after it converged to its steady state. **Settling area** is employed as a measure of disturbance rejection in this work, thanks to the simplification of our model [29]. Specifically, as depicted in figure 4, it indicates the total of the areas enclosed between two steady-state boundary lines and actual trajectory outside the steady-state region. This measure provides an intuitive identification regarding how much area is in departure from the undisturbed route due to the perturbation. Of particular note is that the parallel elasticity modelled in this paper is defined position-dependent, and naturally the settling area values are expected to vary as the perturbed positions. To deal with this issue, we sample the settling area data at 10°, turning points calculated by $C_L/2C_{NL}$ when $C_{NL} < 0$ and 50° (see figure 3) to approximate the disturbance rejection levels at different joint positions. To facilitate analysis, the turning points were restricted in the range of [20°, 40°] in the subsequent simulations through limiting $C_L \in [2\pi/9, 4\pi/9] \cdot C_{NL}$.

2.3.2. Energy efficiency

In the second stage, the joint was commanded to execute the same motion. In order to maintain this motion, the two unidirectional motors have to offer a certain contribution, in collaboration with the passive elastic elements. The second key performance criterion in this work is therefore energy efficiency. Inspired by the criterion of cost of transport (CoT) [30], which has widely used to quantitate the energy cost of humans, animals and robots of different sizes, here we adopt **angular cost of transport** (A-CoT) to describe the energy dissipated by the joint per unit radian, defined as

$$A-\text{CoT}\,|_{\Theta} = \frac{\int \tau_{\text{M}} \cdot \mathrm{d}\Theta}{mgLd_{\Theta}}, \tag{4}$$

where m, L and g denote the mass, length of the lower joint link and gravitational acceleration. τ_{M} is the active torque fed into the joint to the maintain the motion Θ, while d_{Θ} represents the total angular displacement of Θ. Such definition characterizes the average energy cost of the joint during, for example, one motion period. Seeking a good correspondence with the disturbance rejection defined above, we further refine the A-CoT to a specific position level by modifying the definition as

$$A-\text{CoT}\,|_{\theta} = \frac{\int \tau_{\text{M}} \cdot \mathrm{d}\theta}{mgL \cdot 4\Delta\theta}, \tag{5}$$

where τ_{M} is the corresponding active torque when the joint goes through θ within a motion period (e.g. from $(\theta + \Delta\theta)$ to $(\theta - \Delta\theta)$ and back from $(\theta - \Delta\theta)$ to $(\theta + \Delta\theta)$), $\Delta\theta$ is infinitely small (set to1° in this paper). Such definition not only helps understand the position-dependent elasticity profile, but, more importantly, enables the subsequent trade-off analysis between disturbance rejection and energy efficiency. Similar to the disturbance rejection behaviour, the energy efficiency levels at 10°, turning points and 50° are sampled. Note that the A-CoT here is actually a different measure and not comparable with the commonly used CoT.

3. Results

It can be seen from equation (1) that the addition of parallel elasticity changes the dynamics of the joint system. In this section, we show how and to what extent it affects the disturbance rejection and energy efficiency behaviours. To facilitate analysis, we restrict the turning locations of $C_{\text{NL}} < 0$ to the range of [20°, 40°].

3.1. Effect of parallel elasticity on disturbance rejection

In figures 5(a)–(c) the results of the first simulation stage are presented. The plots show the disturbance rejection level using settling area measure when the joint is equipped with parallel elasticity of various configurations. It can be seen that parallel elasticity has a roughly positive effect, with the exception of the situation of $C_{\text{NL}} < 0$ at the location of 50° (figure 5(c)), although different trends are exhibited across locations. Specifically, at the location of 10°, the disturbance rejection behaviour is continuously improved with increasing linear coefficient C_{L}, suggesting that for scenario 2 of linear elasticity, a high stiffness is preferable. Such preference essentially leads to the superiority of $C_{\text{NL}} > 0$ to $C_{\text{NL}} < 0$, because for a certain C_{L}, a positive C_{NL} increases the effective stiffness. Due to the underlying constraint that a muscle can only generate a pulling force but not a pushing force, the lower bound of C_{NL} is limited, but one can infer that a degrade may appear with C_{NL} less than a certain value. The changes during the turning region are slight, between $-3\% \sim 4\%$ (figure 5(b)). At the location of 50°, the tendencies of disturbance rejection behaviour relative to C_{L} and C_{NL} are the same with those at the location of 10°, but with a steeper slope over C_{NL}. Surprisingly, a completely negative effect is observed for scenario 3 with $C_{\text{NL}} < 0$. Although with increasing C_{L} parameter, the disturbance rejection behaviour enhances as well, it seems that C_{NL} may be more crucial than C_{L} in terms of disturbance rejection behaviour at the location of 50°, as adjusting C_{L} can only reduce but not reverse the negative influence.

3.2. Effect of parallel elasticity on energy efficiency

Figures 5(d)–(f) shows the results of the second simulation phase, that is, the influence of parallel elasticity on energy efficiency. The first interesting finding observed is that the energy consumption increases with linear coefficient C_{L} and nonlinear coefficient $|C_{\text{NL}}|$, with the exception of the tiny area marked by black dots in figure 5(f). Similar effects occur across locations, but become more significant for $C_{\text{NL}} > 0$ and less significant for $C_{\text{NL}} < 0$ as position θ increases. This is the most fundamental result suggesting that the energy efficiency property can have a slight improvement (no more than 3%) only at the location of 50° with elasticity of $C_{\text{NL}} < 0$ and small C_{L}, otherwise, introducing elasticity in parallel to actuators would likely have a negative effect on energy efficiency. By comparing the changing trends in A-CoT values at the location of 10° (d), one can see that energy efficiency depends to a large extent on the coefficient C_{L}, as the A-CoT values only have a slight change when fixing C_{L} and varying C_{NL}. Conversely, energy efficiency tends to be highly sensitive to C_{NL} at the location of 50° (f). Particularly, the energetic level deteriorated rapidly when $C_{\text{NL}} > 0$, with a rate of up to 40%. Moreover, another comparison across locations shows that, as position θ goes up, the negative influence of parallel elasticity when

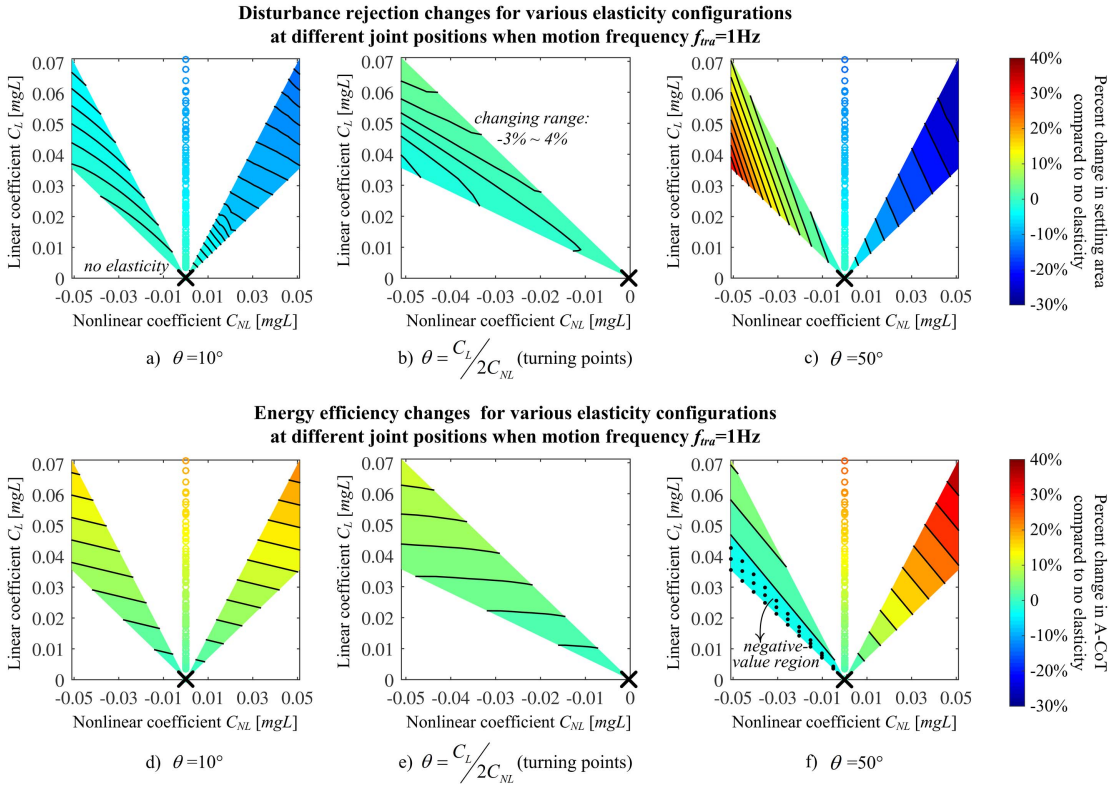

Figure 5. Percent change in disturbance rejection and energy efficiency at different joint positions, compared to the case of no elasticity. The motion frequency is $f_{tra} = 1$ Hz and the parameter space is $C_{NL} \in [-0.05,0.05] \cdot mgL$ and $C_L \in [2\pi/9, 4\pi/9] \cdot C_{NL}$. The black solid curves are the equal-A-CoT (or settling area) lines. The corresponding performance indexes for the case of no elasticity are indicated by the black crosses. The black dots in (f) represent the region where reduced energy cost is observed.

$C_{NL} < 0$ decreases while the influence for $C_{NL} > 0$ tends to be even more significant.

4. Explanation of the behavioural changes: a frequency-domain view

We showed a series of changes in energy efficiency and disturbance rejection behaviours of the joint, resulting from the addition of various profiles of parallel elasticity. From an overall perspective, introducing elasticity in parallel to actuators would probably have a negative effect on energy efficiency, with the exception of the tiny area marked by dots in figure 5(f). An intuitive explanation for this result is the increased difference in frequency between motion trajectory and the joint system. The frequency of motion trajectory used during simulation is 1 Hz, lower than the resonance frequency of the joint itself which non-linearly depends on joint position, from ~1.93 Hz at 10° down to ~1.80 Hz at 60°. In this circumstance, if parallel elasticity is integrated, the resonance frequency of the joint system will be enhanced, thereby expanding the frequency difference. Consequently, a different amount of active contribution is required to compensate such a difference caused by parallel elasticity.

For a more detailed insight, we also examined the mechanical impedance of the synthetic joint system, a central property characterizing the intrinsic dynamics of mechanical systems, which is defined as the ratio of the applied torque to the resultant angular velocity:

$$Z(w) = \frac{\tau_M(jw)}{\dot{\theta}(jw)}. \quad (6)$$

By changing the joint mechanical impedance, the relationship between the angular trajectory of the joint and the net muscle torque required to produce it is correspondingly changed. The effect is illustrated in figure 6, which plots the magnitude and phase of the mechanical impedance as a function of frequency, for a set of C_L, C_{NL} combinations, at different joint positions. The parallel elasticity indeed causes different degrees of change in natural frequencies at the locations of 10° and 50° (figures 6(a)–(c)), confirming the natural frequency-based explanation above. At a closer look, the change of natural frequency is found to be accompanied by a shift of the whole mechanical impedance curve toward the direction of frequency change, thereby leading to the corresponding change in magnitude of mechanical impedance. This gives a more fundamental explanation for energy efficiency behaviours in figure 5, since, obviously, the higher the magnitude of mechanical impedance the more energy is required in order to achieve the same motion. For example, at 1 Hz, compared to the case of no elasticity, there is a slight increase in the magnitude of mechanical impedance at the location of 10° when parallel

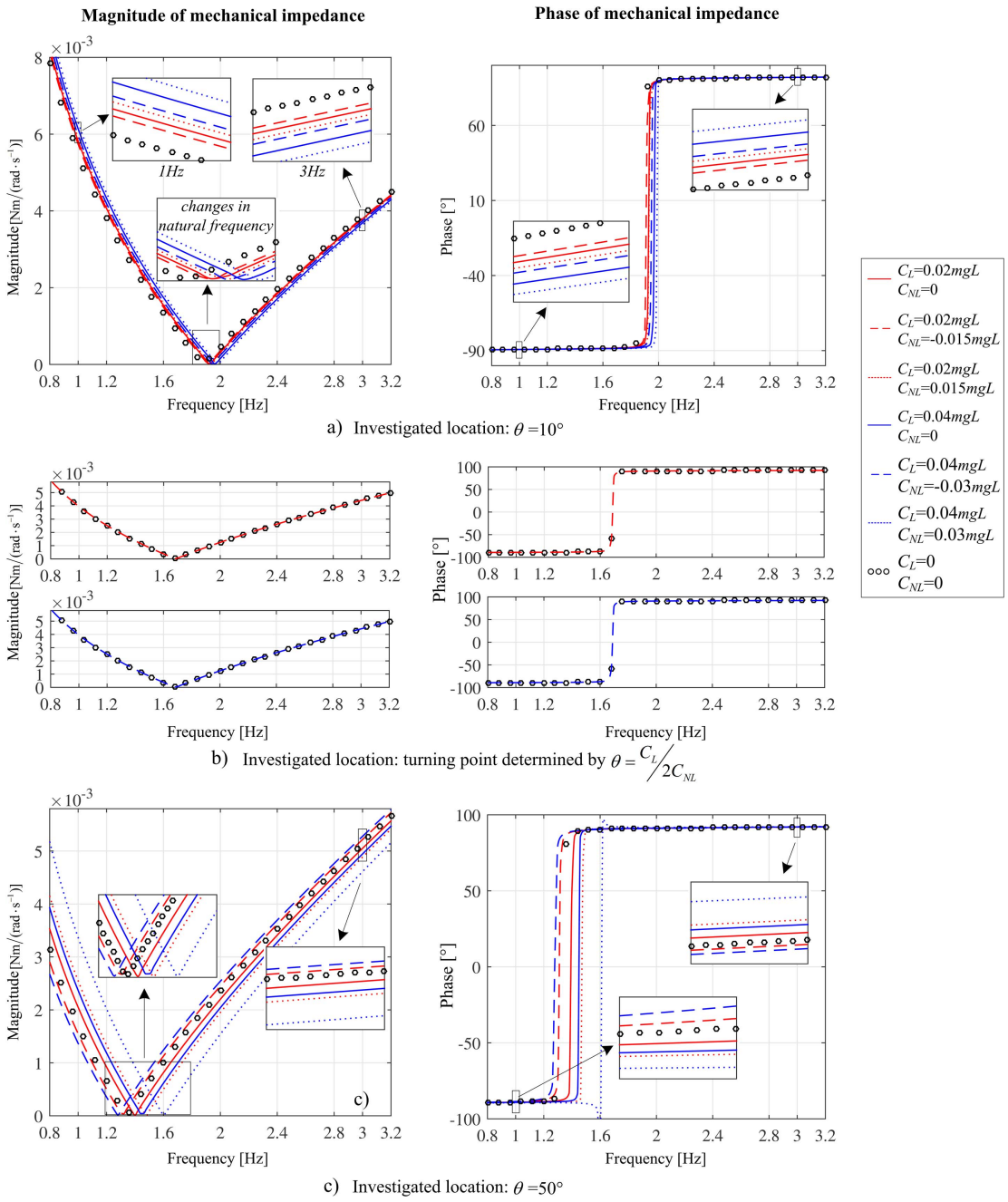

Figure 6. Magnitude (left column) and phase (right column) of the joint mechanical impedance as a function of motion frequency for a set of C_L, C_{NL} combinations, at different joint positions. Insets show enlargements of the boxed areas.

elasticity is applied. This slight increase results in the small rise of energy cost (figures 5(d) and 6(a)). Again, one can see that the mechanical impedance curves with and without parallel elasticity almost overlap at each turning location, corresponding to the result that there is little change in energy efficiency when parallel elasticity is integrated at these points (figures 5(e) and 6(b)). The slight difference in A-CoT in figure 5(e) is due to the fact that A-CoT is calculated as an average of adjacent data of the locations. Likewise, the more significant increase in the magnitude of mechanical impedance provides the most consistent explanation of the energy efficiency behaviour at the location of 50° (figures 5(f) and 6(c)). Particularly, the slight decrease in mechanical impedance found for part of the parameter combinations when $C_{NL} < 0$ provides a mechanistic explanation for the phenomenon in figure 5(f) (the dotted area) that energy efficiency counterintuitively improves.

To interpret the changes in disturbance rejection behaviour, we first look at what determines the settling area that we use as a measure. By the definition in section 2.3, two aspects are involved: (i) deviation magnitude, which denotes the degree of departure of the joint from the undisturbed route due to perturbation, and (ii) response delay, describing how fast the subsequent motor torque would counteract the deviation in case it occurs. The first factor, deviation

magnitude, is inversely proportional to the magnitude of mechanical impedance, since clearly, given a perturbation, the higher the magnitude of mechanical impedance, the less the joint would deviate. Together with the impedance magnitude shown in the left column of figure 6, we can validly infer the change in the deviation magnitude. In terms of response delay, we look at the phase plot of mechanical impedance for a quantitative analysis. A negative impedance phase means the active torque lags the joint velocity, thus a certain time is needed for the subsequent motor torque to react once derivation takes place. In contrast, a positive phase indicates that the active effort is in leading position. Such phase lead enables the subsequent motor torque to play a role when deviation is occurring, and is thus equivalent to enhancing the capability of resistance to perturbation. Referring to figure 6, we can identify how various elasticity configurations affect the disturbance rejection.

So far we have revealed the individual contributions of deviation magnitude and response delay to disturbance rejection. However we still do not have a conclusive answer as to their collective effect, since contradictory trends always appear with them. In fact, it is difficult to establish a mathematical correlation between them due to the high nonlinearity of the problem. But the numerical results in figures 5(a)–(c) and 6 imply that the ability to resist deviation from the start of it occurring seems to be a key. Specifically, according to the above analysis, such resistance of deviation is directly reflected in increased magnitude and advanced phase of the mechanical impedance. For example, at 1 Hz, although the amount of phase lag with parallel elasticity increases at the location of 10° (figure 6(a)), the increased impedance magnitude (figure 6(a)) enhances the resistance to perturbation at the very beginning, even in the whole deviation process, and thereby improves the disturbance rejection (figure 5(a)). The virtually unaltered impedance magnitude and phase (figure 6(b)) correspond to the fact that the settling area changes little at the turning locations (figure 5(b)). As another example, at the location of 50°, despite less phase lag for the parameter combinations when $C_{NL} < 0$ (figure 6(c)), which indicates a reduced response delay, a sharp increase in settling area (figure 5(c)) is still observed. This is because the corresponding magnitude of mechanical impedance (figure 6(c)) is reduced, causing a decrease in the ability to prevent deviation at the initial moment.

To further test the above explanation and extrapolation, we investigate the behavioural changes by letting the joint move at a frequency of 3 Hz. The magnitude and phase data of mechanical impedance can be found again in figure 6, and the observed results are demonstrated in figure 7. We found that the energy efficiency behaviours can be well explained by the corresponding impedance magnitude, exhibiting an inverse correlation. As for the disturbance rejection, the trend is not sensible with small C_{NL}, because the amount of increase in phase lead is not significant and neutralized by the lowered impedance magnitude. But with nonlinear coefficient C_{NL} increasing, the improvement in phase lead becomes significant. As a result, visible enhancements are seen, supporting the aforementioned extrapolation.

5. Discussion

5.1. Linear versus concave versus convex profiles

The profile of parallel elasticity plays a significant role in the behavioural changes. Linear profiles are the most commonly used type thanks to their ease of modelling and physical implementation. Nonlinear profiles are supposed to be more beneficial than linear ones, but it is still not clear what type of nonlinearity makes sense, concave or convex? On the other hand, we have shown in the above sections that parallel elasticity essentially exerts competitive influences on energy efficiency and disturbance rejection, no matter what the elasticity profile is. This implies a trade-off problem when considering the elasticity profiles.

Aiming at capturing this trade-off, we further examine the trade-off plots of settling area against A-CoT at different joint positions and motion frequencies, as illustrated in figure 8. Similarly, the coefficients of elasticity profiles are varied in the range of $[-0.05,0.05] \cdot mgL$ for C_{NL} and $[2\pi/9, 4\pi/9] \cdot C_{NL}$ for C_L. As can be seen, each subfigure consists of a solid curve (grey in (a), (c), (d), (f) and coloured in (b), (e)), which corresponds to the trade-offs occurring with linear elasticity profiles ($C_{NL} = 0$), and two regions separated by the curve, which summarize the trade-offs of $C_{NL} > 0$ and $C_{NL} < 0$, respectively. For the case of low frequency (figures 8(a)–(c)), it is interesting to observe that the corresponding trade-offs obtainable with $C_{NL} > 0$ are always located at the lower part of the base line, while the trade-off points with $C_{NL} < 0$ lie in the upper side. According to the definitions of settling area and A-CoT, such distribution patterns mean that the concave type of elasticity profile is able to achieve a more advantageous balance compared to the convex and linear ones—that is, improving one objective while deteriorating the other one less.

Similarly, consistent distribution trends are observed when the joint moves at 3 Hz (figures 8(d)–(f)), indicating that concave profiles are also superior to the other two types in the high-frequency mode. At a closer look, we can find that concave profiles are particularly beneficial for those robots where energy cost is a factor. At the joint location of 50°, the energetic level is significantly worsened (approximately 0.1 at 10° compared to 0.7 at 50°), and unfortunately the enhancement in terms of energy efficiency thus gained by exploiting convex elasticity is extremely limited, no more than 4% (from 0.77 to 0.74, see figure 8(f)). Conversely, if concave elasticity is employed, energy

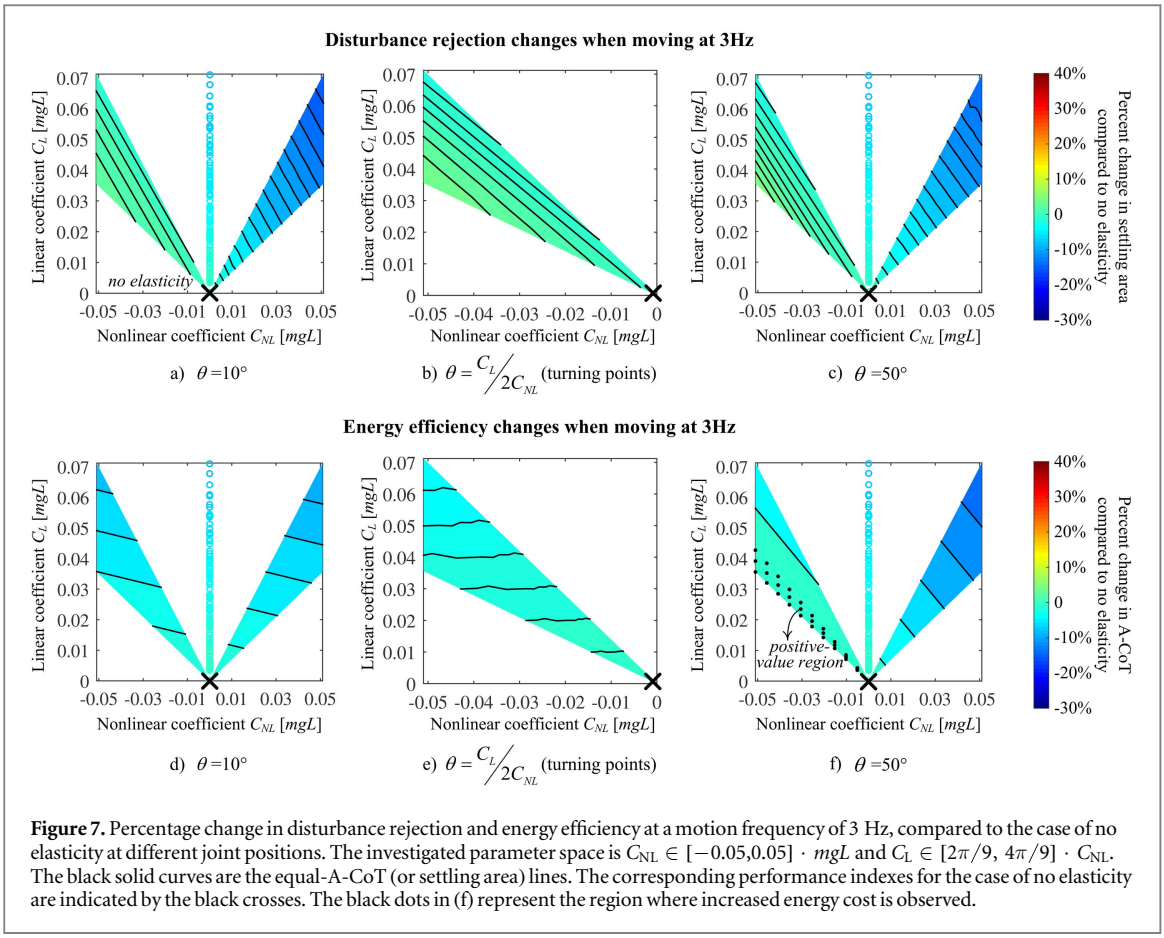

Figure 7. Percentage change in disturbance rejection and energy efficiency at a motion frequency of 3 Hz, compared to the case of no elasticity at different joint positions. The investigated parameter space is $C_{NL} \in [-0.05,0.05] \cdot mgL$ and $C_L \in [2\pi/9, 4\pi/9] \cdot C_{NL}$. The black solid curves are the equal-A-CoT (or settling area) lines. The corresponding performance indexes for the case of no elasticity are indicated by the black crosses. The black dots in (f) represent the region where increased energy cost is observed.

efficiency would be expected to improve by up to roughly 13% (from 0.75 to 0.65), without sacrificing much of the disturbance rejection property. Moreover, we note that Mahdi Khoramshahi *et al* [18] found that a spinal joint with piecewise linear elasticity, essentially a simple variation of the concave elasticity, is able to achieve a better balance between energy efficiency and speed than purely linear ones in quadrupedal locomotion. Such trade-off analysis above also provides a likely explanation as to why biological systems have a similar muscular elasticity characteristic (see figure 1).

5.2. Reducing the downside of parallel elasticity

We showed that employing parallel elasticity would inevitably introduce unwanted side effects. These negative consequences can be reduced or even avoided by proper designs. To facilitate analysis, the equilibrium point of parallel elasticity in our model is assumed at 0°, making the elastic torque always in the same direction as gravitational torque. Hence, the first possible way is to include an offset in the equilibrium position of parallel elasticity [16]. By choosing the correct offset, it will be possible to recycle the negative work done by gravity, thereby improving the energy efficiency of active efforts. Another common design technique is to add (active or passive) clutches into the joint structure, which will allow decoupling of the parallel elasticity when not desired [31]. Note that this method may require additional mechatronic designs that may complicate the structure. However, we do not discuss the details here.

5.3. Application to artificial systems

As identified in the previous sections, our main finding is the benefit of muscle-like concave elasticity characteristics for overcoming the trade-off between energy efficiency and disturbance rejection during joint rotating. The result is able to contribute to the design of rotary actuator units or robotic joints, thereby helping to enhance the performance of articulated systems such as robotic limbs and prostheses. This improvement in hardware design is particularly useful for those systems where both energy cost and robustness are factors. For example, this would be the case for a legged robot needing to locomote in highly rugged terrains with power autonomy [2, 32]. Such scenarios typically occur in applications such as search and rescue and planetary exploration. Another example would be robotic hands that need to achieve energy-efficient and robust grasping and manipulation [15]. By reasonably integrating identified elasticity characteristics into their joints, the performance of these systems is expected to be enhanced. In addition, since the improvement is obtained purely from the self-adjustment of joint

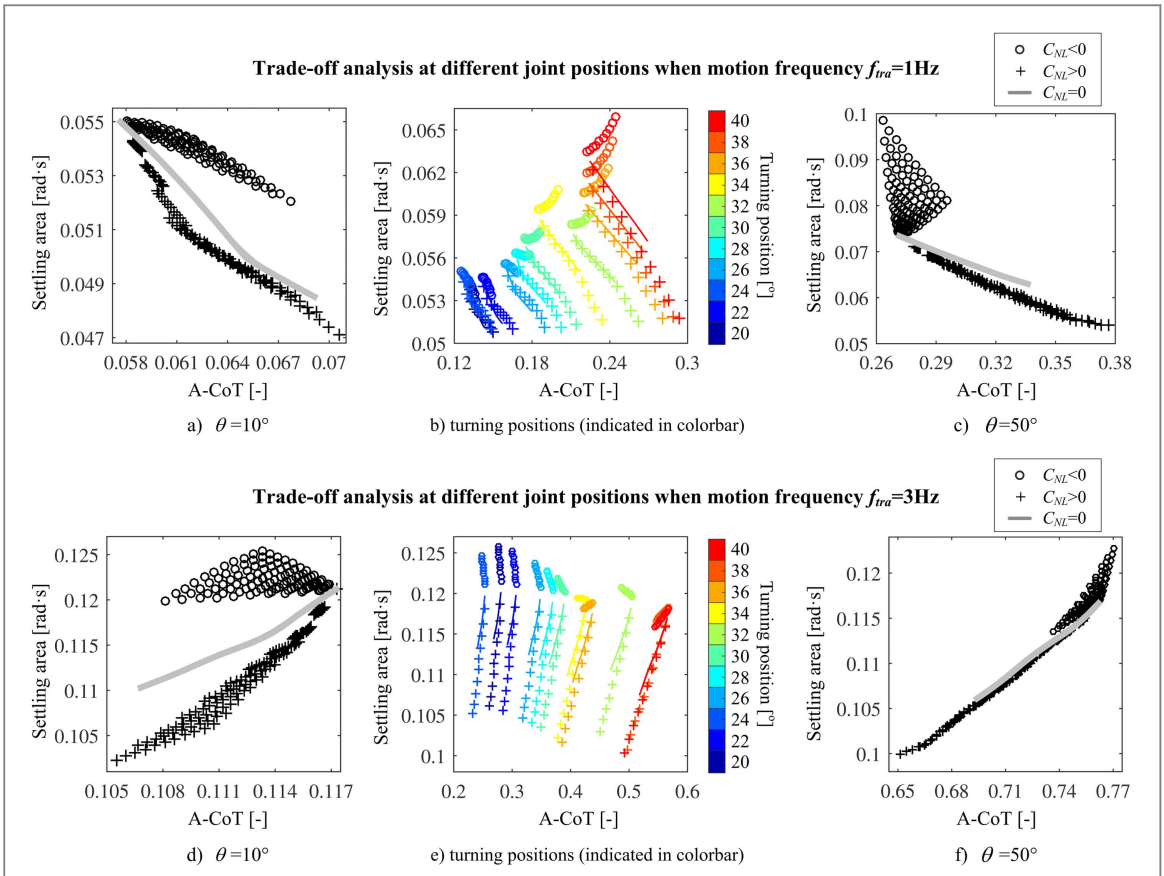

Figure 8. Trade-off plots between energy efficiency and disturbance rejection for the parameter space of $C_{\mathrm{NL}} \in [-0.05, 0.05] \cdot mgL$ and $C_{\mathrm{L}} \in [2\pi/9, 4\pi/9] \cdot C_{\mathrm{NL}}$ at different joint positions, when the joint moves at low-frequency (1 Hz) and high frequency (3 Hz). The colours correspond to different turning points calculated by $\theta = C_{\mathrm{L}}/2C_{\mathrm{NL}}$, as indicated in the colour bars. Circles: data obtained when $c_{\mathrm{NL}} < 0$. Plus signs: trade-offs obtained when $c_{\mathrm{NL}} > 0$. Solid lines (grey in (a), (c), (d), (f) and coloured in (b), (e)) represent trade-off curves obtained when $c_{\mathrm{NL}} = 0$.

dynamics, it may also help reduce the dependence and burden of active control.

In order to implement identified parallel elasticity properties in a robotic joint, many design proposals for nonlinear elasticity can be utilized. For example, Kim and Deshpande [33] presented a design methodology for nonlinear stiffness by using a non-circular pulley-spring mechanism. With the synthesis procedure they reported, the shape of the non-circular pulley can be obtained for a desired elasticity profile. Schmit and Okada [34] presented a non-circular cable spool mechanism to synthesize a nonlinear rotational spring. Depending on the shape of the spool, various torque–angle relationships can be realized. Endo *et al* [35] also proposed a design of a non-circular pulley-spring mechanism to produce the desired nonlinear torque profile. In addition, the linear springs in these mechanisms can be replaced by other compliant materials like rubber and viscoelastic polyurethane, which could make the mechanisms easier to integrat into lightweight and small robots. Representative examples of such designs include those proposed in [36] and [37]. With these clever mechanisms, it is possible to produce various types of elasticity profiles. And as a theoretical reference for hardware designers, the result of this study reveals that concave ones may be more reasonable when designing elasticity in parallel with actuators.

5.4. Towards hardware realization of nonlinear parallel elasticity

While the theoretical results indicated that concave parallel elasticity provides robotic joints with better passive performance, several practical considerations with hardware realization have to be made. First of all, implementing nonlinear elasticity usually needs additional mechanical designs, which leads to high system complexity, e.g. manufacturing and operation. Notably, such a design can add weight and inertia to the system, lowering, in turn, the energy efficiency. In addition, it is unsuitable for small and lightweight platforms to integrate these complex nonlinear mechanisms. On the side of control, the nonlinear property as well as the additional structural components may complicate the modelling, analysis and parameter identification of the whole system. In summary, we have to think about whether or not the performance enhancement outweighs the complexity increase involved in doing so on the side of the overall system.

5.5. Limitations and future work

Although we have shown the superiority of concave parallel elasticity, which agrees well with biological evidence, the use of the presented model has several limitations. As mentioned previously, tendon-like series elasticity was not considered in our model. And because of this, no large impulsive forces (e.g. ground impact at touchdown in legged locomotion) were adopted during simulation, as series elasticity is dominant in impulse absorption. Force–length and force–velocity relations of the active muscle force were simplified as well [38, 39]. Damping variations within muscles were not considered. Consequently, the incomplete mapping caused by such approximations between our conceptual model and biological joints may interfere with the interpretation of other biological principles. In addition to the simplifications inside muscles, the biarticular structure of muscles was also not taken into account. Such structures are argued to contribute to energy efficiency and disturbance rejection of a joint as well. To purely examine the utilization of parallel elasticity, the joint was open-loop controlled during simulations, which may also result in noise to the disturbance rejection metric.

Our future work, therefore, will improve the model accuracy by reasonably removing these approximations. We emphasize 'reasonably', because, despite not providing a faithful correspondence to biological reality, advantages in terms of ease of modelling and reduction of parameter dimensionality were indeed seen in our studies, simplifying data analysis and thereby facilitating the illumination of basic principles. More importantly, our studies are conducted in the context of robotic application, rather than pure biomechanics. We have to think about the transfer of the presented models to robotic prototypes; that is, practical constraints of state-of-the-art technologies. Obviously, a relatively complicated model is challenging for straightforward hardware realization, as discussed above. Apart from improving the joint model, suitable active control is also indispensable if the joint system is put in practical use. Thus, we will also work on developing appropriate control strategies to enhance joint stability and adaptivity.

6. Conclusions

In this work, the effects of parallel elasticity on energy efficiency and disturbance rejection, and the reasons underlying these behavioural changes, are explored with a conceptual joint model. The results may contribute to the design of articulated machines where both energy cost and robustness are factors, such as robotic manipulators working in limited space or legged robots locomoting in highly rugged terrains that need to deliberately swing and place the legs. Several lessons can be learned from this study. First, no not all nonlinear parallel elasticity is superior to linear elasticity. It depends on the type of nonlinearity. In principle, a concave profile is advantageous. Second, natural frequency of a joint system can be altered by parallel elasticity, either increased or decreased depending on the profiles introduced, and matched to specific tasks, for example, high speed moving. Third, the universal elasticity profile exhibited within biological muscles is probably evolved as the result of a trade-off between multiple objectives, among which energy efficiency and disturbance rejection might be two contributing factors.

Acknowledgments

This work was supported in part by the National Natural Science Foundation of China (Grant No. 51105101 and 61473102) and in part by the self-managed project of the State Key Laboratory of Robotics and System in Harbin Institute of Technology (SKLRS200901A01). The authors would like to thank Dr Andre Rosendo for his helpful comments on an earlier version of this article. The first author was also supported by the China Scholarship Council (201406120118).

References

[1] Grebenstein M, Chalon M, Friedl W, Haddadin S, Wimböck T, Hirzinger G and Siegwart R 2012 The hand of the DLR hand arm system: designed for interaction *Int. J. Robot. Res.* **31** 1531–55

[2] Chen J, Liu Y, Zhao J, Zhang H and Jin H 2014 Biomimetic design and optimal swing of a hexapod robot leg *J. Bionic Eng.* **11** 26–35

[3] Alexander R M 2003 *Principles Of Animal Locomotion* (Princeton, NJ: Princeton University Press)

[4] Magid A and Law D J 1985 Myofibrils bear most of the resting tension in frog skeletal muscle *Science* **230** 1280–2

[5] Granzier H L and Pollack G H 1990 The descending limb of the force-sarcomere length relation of the frog revisited *J. Physiol.* **421** 595–615

[6] Altringham J D and Bottinelli R 1985 The descending limb of the sarcomere length-force relation in single muscle fibres of the frog *J. Muscle Res. Cell Motil.* **6** 585–600

[7] Davis J, Kaufman K R and Lieber R L 2003 Correlation between active and passive isometric force and intramuscular pressure in the isolated rabbit tibialis anterior muscle *J. Biomech.* **36** 505–12

[8] Winters T M, Takahashi M, Lieber R L and Ward S R 2011 Whole muscle length-tension relationships are accurately modeled as scaled sarcomeres in rabbit hindlimb muscles *J. Biomech.* **44** 109–15

[9] Gollapudi S K and Lin D C 2009 Experimental determination of sarcomere force-length relationship in type-I human skeletal muscle fibers *J. Biomech.* **42** 2011–6

[10] Zajac F E 1989 Muscle and tendon: properties, models, scaling, and application to biomechanics and motor control. *Crit. Rev. Biomed. Eng.* **17** 359–411

[11] Hutter M, Remy C D, Hoepflinger M A and Siegwart R 2013 Efficient and versatile locomotion with highly compliant legs *IEEE-ASME Trans. Mechatron.* **18** 449–58

[12] Kong K, Bae J and Tomizuka M 2012 A compact rotary series elastic actuator for human assistive systems *IEEE-ASME Trans. Mechatron.* **17** 288–97

[13] Sulzer J S, Peshkin M A and Patton J L 2005 MARIONET: an exotendon-driven rotary series elastic actuator for exerting joint torque *IEEE Int. Conf. Intell. Rehabilitation Robotics. (ICORR) (Chicago, IL)* pp 103–8
[14] Lens T and von Stryk O 2012 Investigation of safety in human-robot-interaction for a series elastic, tendon-driven robot arm *IEEE/RSJ Int. Conf. Intell. Robots Sys. (IROS) (Vilamoura, Portugal)* pp 4309–14
[15] Niehues T D, Rao P and Deshpande A D 2015 Compliance in parallel to actuators for improving stability of robotic hands during grasping and manipulation *Int. J. Robot. Res.* **34** 256–69
[16] Migliore S A, Ting L H and DeWeerth S P 2010 Passive joint stiffness in the hip and knee increases the energy efficiency of leg swinging *Auton Robot* **29** 119–35
[17] Yang T, Westervelt E R, Schmiedeler J P and Bockbrader R A 2008 Design and control of a planar bipedal robot ERNIE with parallel knee compliance *Auton Robot* **25** 317–30
[18] Khoramshahi M, Bidgoly H J, Shafiee S, Asaei A, Ijspeert A J and Ahmadabadi M N 2013 Piecewise linear spine for speed–energy efficiency trade-off in quadruped robots *Robot. Auton. Syst.* **61** 1350–9
[19] Karssen J G D and Wisse M 2011 Running with improved disturbance rejection by using non-linear leg springs *Int. J. Robot. Res.* **30** 1585–95
[20] Migliore S A, Brown E A and DeWeerth S P 2007 Novel nonlinear elastic actuators for passively controlling robotic joint compliance *J. Mech. Design* **129** 406–12
[21] Hill A V 1938 The heat of shortening and the dynamic constants of muscle *Proc. R. Soc. Lond.* B **126** 136–95
[22] Latash M L and Zatsiorsky V M 1993 Joint stiffness: myth or reality? *Hum. Mov. Sci.* **12** 653–92
[23] Hwang W, Kelly N G and Boriek A M 2005 Passive mechanics of muscle tendinous junction of canine diaphragm *J. Appl. Physiol.* **98** 1328–33
[24] Herbert R D and Crosbie J 1997 Rest length and compliance of non-immobilised and immobilised rabbit soleus muscle and tendon *Eur. J. Appl. Physiol.* **76** 472–9
[25] Millard M, Uchida T, Seth A and Delp S L 2013 Flexing computational muscle: modeling and simulation of musculotendon dynamics *J. Biomech. Eng.* **135** 021005
[26] Marques H G, Bharadwaj A and Iida F 2014 From spontaneous motor activity to coordinated behaviour: a developmental model *PLoS Comput. Biol.* **10** e1003653
[27] Dickinson M H, Farley C T, Full R J, Koehl M A R, Kram R and Lehman S 2000 How animals move: an integrative view *Science* **288** 100–6
[28] Roberts T J and Azizi E 2011 Flexible mechanisms: the diverse roles of biological springs in vertebrate movement *J. Exp. Biol.* **214** 353–61
[29] Miller B, Schmitt J and Clark J E 2012 Quantifying disturbance rejection of SLIP-like running systems *Int. J. Robot. Res.* **31** 573–87
[30] Tucker V A 1975 The energetic cost of moving about: walking and running are extremely inefficient forms of locomotion. Much greater efficiency is achieved by birds, fish—and bicyclists *Am. Sci.* **63** 413–9
[31] Collins S H, Wiggin M B and Sawicki G S 2015 Reducing the energy cost of human walking using an unpowered exoskeleton *Nature* **522** 212–5
[32] Hutter M, Gehring C, Hopflinger M A, Blosch M and Siegwart R 2014 Toward combining speed, efficiency, versatility, and robustness in an autonomous quadruped *IEEE Trans. Robot.* **30** 1427–40
[33] Kim B and Deshpande A D 2014 Design of nonlinear rotational stiffness using a noncircular pulley-spring mechanism *J. Mechanisms Robot.* **6** 041009
[34] Schmit N and Okada M 2012 Design and realization of a non-circular cable spool to synthesize a nonlinear rotational spring *Adv. Robot.* **26** 234–51
[35] Endo G, Yamada H, Yajima A, Ogata M and Hirose S 2010 A passive weight compensation mechanism with a non-circular pulley and a spring *IEEE Int. Conf. on Robotics and Automation (ICRA) (Anchorage, Alaska)* pp 3843–8
[36] Schepelmann A, Geberth K A and Geyer H 2014 Compact nonlinear springs with user defined torque-deflection profiles for series elastic actuators *IEEE Int. Conf. on Robotics and Automation (ICRA)* (Hong Kong, China) pp 3411–6
[37] Kuo P-H and Deshpande A D 2015 A novel joint design for robotic hands with human-like nonlinear compliance *J. Mechanisms Robot.* **8** 021004
[38] Haeufle D, Grimmer S and Seyfarth A 2010 The role of intrinsic muscle properties for stable hopping—stability is achieved by the force–velocity relation *Bioinsp. Biomim.* **5** 016004
[39] Schmitt S, Haeufle D, Blickhan R and Günther M 2012 Nature as an engineer: one simple concept of a bio-inspired functional artificial muscle *Bioinsp. Biomim.* **7** 036022